

Spontaneous locomotion of phoretic particles in three dimensions

Wei-Fan Hu ¹, Te-Sheng Lin ², Salima Rafai ³ and Chaouqi Misbah ³

¹*Department of Mathematics, National Central University, Taoyuan 32001, Taiwan*

²*Department of Applied Mathematics, National Yang Ming Chiao Tung University, Hsinchu 30010, Taiwan*

³*LIPhy, CNRS, Université Grenoble Alpes, 38000 Grenoble, France*



(Received 31 May 2021; accepted 1 March 2022; published 17 March 2022)

The motion of an autophoretic spherical particle in a simple fluid is analyzed. This motion is powered by a chemical species which is absorbed or emitted by the particle and which diffuses and is advected in the surrounding fluid. The transition from the nonmotile to the motile state occurs if the Péclet number Pe (defined as the ratio of the solute emission rate over the solute diffusion rate) is sufficiently large. We first analyze the axisymmetric case (restricting the particle to a unique direction). In this case, we find that the motion of the particle transits from a motionless to a directed motion at a given critical Pe . Increasing Pe , we find a second critical value where the particle becomes stagnant in a symmetric flow. A further increase of Pe leads to a recovery of motile motion. When Pe is increased even further, the particle shows a periodic motion undergoing a subharmonic cascade before entering chaos. In this regime, the mean-square displacement behaves quadratically with time (a ballistic regime). When the axisymmetry constraint is relaxed, allowing the particle to freely move in three-dimensional space, we find that at a small Pe the particle moves in a straight manner. There exists a critical value where the particle exhibits an oscillatory motion with a meandering trajectory. Increasing Pe further leads to chaotic bursts for some time, before entering fully into chaos via the intermittency scenario at a critical Pe number. In this regime, the particle shows run-and-tumble-like dynamics: The trajectory is then characterized by a ballistic swimming nature at a short time and a diffusive nature at a long time.

DOI: [10.1103/PhysRevFluids.7.034003](https://doi.org/10.1103/PhysRevFluids.7.034003)

I. INTRODUCTION

It has now become clear that many living systems, including prokaryotic [1,2] and eukaryotic [3–6] cells, have the ability to swim in a fluid by deploying several strategies such as flagella [7–11] and cilia beating [12] and ample shape deformation (amoeboid swimming) [4,6,13–17]. Other motile systems use, instead of body deformation, chemical activity in order to move forward. Typical examples are Marangoni-driven particles [18–20] (e.g., drops, also referred to as phoretic particles). In this case, the particle emits or absorbs a chemical that induces a Marangoni flow due to the fact that surface tension depends on the chemical concentration.

An outstanding feature of these systems is their ability to exhibit a variety of trajectories including straight, circular, helical, and chaotic motion. It has actually been known for more than a century that the movement of living entities (such as zoospores and flagellated or ciliated Protista) follows complex trajectories, such as spiral ones [21]. More recently, several studies have reported on complex trajectories of real and artificial microswimmers [12,22–29]. The identification of the minimal ingredients for the occurrence of complex trajectories has become a major issue. Ingredients, such as particle asymmetry [25], and the complex nature of the suspending fluid [27] have led to the discovery of curved trajectories (e.g., helical and spiral). At the same time, numerical

simulations in two dimension have shown the occurrence of curved and chaotic trajectories even for a circular phoretic particle moving in a simple fluid and in the absence of noise [29]. Recently, a general theory [30,31], based on symmetry arguments, has shown that circular, helical, and chaotic trajectories should emerge for any symmetric particles (sphere) powered by a concentration field moving in an isotropic medium (e.g., simple fluid). The theory states that these motions are generic, but this does not mean that for a given active system these trajectories will actually manifest. Indeed, since the theory is based on symmetries, it does not provide information on the region of parameter space where such motion is expected. To achieve this goal one needs to focus on a given system by analyzing explicitly the corresponding model. The present work is directed towards this objective. Our aim here is to deal with a fully nonaxisymmetric three-dimensional (3D) swimming problem, which reveals several different features in comparison to the axisymmetric situation. As a preliminary study, we will first focus on an axisymmetric model and compare our results to those of [19].

We are inspired by systems of water droplets in oil and surfactant phases [28]. It was proposed for such systems that the transition from the nonmotile to a motile state is driven by (i) tangential velocity driven by a concentration gradient along the surface and/or (ii) a Marangoni effect due to the dependence of surface tension on the concentration. In the present paper we consider a rigid spherical particle so that the effect of surface tension does not play a role, and we focus on the motility due to tangential transport only.

In [19] a numerical study of axisymmetric motion in three dimensions reported on several motions. Besides a straight motion where the speed is a constant, two other motions were reported for higher Péclet number (denoted by Pe), namely, a stationary particle solution with a symmetric extensional flow and a chaotic regime where the particle moves back and forth in an erratic manner. In this regime the motion is ballistic, that is, the mean-square displacement (MSD) \mathcal{D} behaves with time τ as $\mathcal{D} \sim \tau^2$. That work also reported that chaotic oscillations may not arise for pure Marangoni propulsion and that a small amount of diffusiphoretic behavior is needed. We have analyzed [29] numerically a phoretic model (including tangential transport, but with no Marangoni effect) in two dimensions and have shown that with increasing Péclet number we have a successive motion from straight motion to meandering, circular, and chaotic trajectories. In the chaotic regime $\mathcal{D} \sim \tau^2$ at short times and $\mathcal{D} \sim \tau$ at longer times, that is, the particle exhibits a persistent random-walk motion. More recently, Chen *et al.* [32] considered theoretically and numerically two situations: (i) a solid particle having an extended planar geometry and (ii) a 3D spherical particle. In the first case, besides the straight steady motion, they reported on the emergence of multiple concentration plumes from the catalytic plane, which eventually merge into a single larger one when Pe is large enough. For a spherical particle, they found that, besides a straight motion, plumes are generated at the surface of the particle, which starts to move irregularly, without providing the scenario by which irregular motion takes place or analyzing the resulting trajectory. Recent experiments by Hokmabad *et al.* [33] focused on the motion of an oil droplet suspended and slowly dissolving in supramicellar aqueous solutions of ionic surfactants, using a Hele-Shaw geometry (quasi-2D motion). The Péclet number was increased due to a modification of the viscosity of the suspending solution. A remarkable feature is that the particle undergoes, at high enough Pe , a chaotic motion in the form of a self-avoiding random walk. Self-avoidance of trajectories in confined quasi-2D geometry was also reported in another experiment of autophoretic particles (similar in principle to the above-described system) [34]. Another experimental study [35] focused on droplets of diethyl phthalate (DEP) suspended in an aqueous solution of sodium dodecyl sulphate. The resulting DEP swollen micelles are thermodynamically more stable than the empty ones. It is argued that an infinitesimal perturbation in the velocity of the droplet leads to an anisotropy in surfactant concentration. This asymmetry induces a Marangoni stress that forces the surface flow of surfactants, leading to a spontaneous droplet motion. By adding surfactants in the solution, various drop motions are analyzed. As the surfactant concentration increases, the motion turns from a regular straight motion into an irregular one, with a ballistic motion at short times and a diffusive one at long times, in agreement with our

previous 2D simulation [29]. This experiment [35], in contrast to the two others [33,34], did not report on self-avoiding trajectories. This question will be discussed further in this paper.

None of the above theoretical or numerical studies analyzed in detail how chaotic motion takes place or the chaotic characteristics of the motion. These questions constitute a main contribution of the present work. A systematic numerical investigation of the system shows a variety of motions from straight to meandering to chaotic, as well as swimming stagnation. We will first focus on the simplified case where an axisymmetry constraint is imposed and show that the particle can swim beyond a critical Péclet number. In this regime, a cometlike solute concentration field takes place; the solute shows a polarity. By increasing Pe the particle can be arrested, due to the symmetric bipolarization of the solute pattern. A further increase of Pe leads to a subharmonic cascade of the particle position, before exhibiting chaos, in agreement with the study in [19]. In contrast to that study, by looking more closely at the chaotic motion, we show here that this motion can be split into two ballistic regimes, one at short enough times and one at long times. The two regimes have two different amplitudes of their MSD and we will provide an intuitive understanding of these two regimes. In addition, we analyze here in detail the transition towards chaos and show that it occurs via a subharmonic cascade. We analyze here also the nonaxisymmetric case in great detail. We find in this case meandering and chaotic motion and this time via an intermittency scenario.

This paper is organized as follows. In Sec. II we describe the mathematical model for the diffusiophoretic system and derive the analytical solution of the velocity field. We further analyze the linear stability of the trivial stationary solution of the immobile state and determine the onset of stability. A systematical numerical investigation of the problem in axisymmetric and fully three-dimensional space is presented in Sec. III. Concluding remarks and prospects for future work are addressed in Sec. IV.

II. MODEL

A spherical colloidal particle of radius a is suspended in a Newtonian solvent of viscosity η and density ρ , where a chemical species dispersed in the solution interacts with the particle through an *isotropic* chemical activity \mathcal{A} at the particle surface. We focus on the so-called sharp interface limit, in which the length λ , which characterizes the interaction potential between the chemical species and the particle, is much smaller than a . In this regime, a local slip flow is created along the particle surface, leading to a phoretic motion along with a net flow field [18]. The concentration of the solute diffuses with diffusivity D and is advected by the surrounding fluid flow.

To proceed, we nondimensionalize the length, fluid velocity, and concentration as in [18] by the characteristic values a , $|\mathcal{A}\mathcal{M}|/D$, and $a|\mathcal{A}|/D$, respectively. Here the signed mobility $\mathcal{M} = \pm k_B T \lambda^2 / \eta$, which depends on the particle-solvent interaction forces, is defined with the Boltzmann constant k_B and the temperature T . We assume the fluid inertia is negligible as supported by the typical diffusiophoretic experiments [36] in which the Reynolds number $\text{Re} = \rho |\mathcal{A}\mathcal{M}| a / \eta D$ is generally small ($\text{Re} \sim 10^{-5}$). Therefore, the motion of the fluid in the body-fixed frame (attached to the center of the particle) obeys the incompressible Stokes equations

$$-\nabla p + \Delta \mathbf{u} = \mathbf{0}, \quad \nabla \cdot \mathbf{u} = 0, \quad (1)$$

where p is the pressure and the velocity is decomposed by $\mathbf{u} = u_r \mathbf{e}_r + u_\theta \mathbf{e}_\theta + u_\phi \mathbf{e}_\phi$ [\mathbf{e}_r , \mathbf{e}_θ , and \mathbf{e}_ϕ denote the standard basis in spherical coordinates (r, θ, ϕ)]. We assume that the fluid variables and the solute concentration, denoted by c , are all defined in an unbounded domain $\Omega = \{(r, \theta, \phi) \mid r \in [1, \infty), \theta \in [0, \pi], \phi \in [0, 2\pi)\}$. The surface slip flow along the particle serves as a boundary condition and is proportional to the tangential gradients of concentration as

$$\mathbf{u}(r=1) = M \nabla_s c(r=1), \quad (2)$$

where $M = \mathcal{M}/|\mathcal{M}| = \pm 1$ is the dimensionless mobility and $\nabla_s = (\mathbf{I} - \mathbf{n} \otimes \mathbf{n}) \nabla$ is a surface gradient operator, with \mathbf{n} the normal vector along the particle surface. In the far-field limit the

velocity field converges to the phoretic propulsion velocity

$$\mathbf{u}(r \rightarrow \infty) = -(\mathbf{U} + \boldsymbol{\Omega} \times \mathbf{r}), \quad (3)$$

where $\mathbf{r} = r\mathbf{e}_r$. The phoretic kinematics of the particle can be found by using the reciprocal theorem [37], which gives the relation for the translational velocity \mathbf{U} and rotational velocity $\boldsymbol{\Omega}$ to the surface slip velocity via the surface integrals over the sphere:

$$\mathbf{U} = -\frac{1}{4\pi} \int \mathbf{u}(r=1) dS, \quad \boldsymbol{\Omega} = -\frac{3}{8\pi} \int \mathbf{e}_r \times \mathbf{u}(r=1) dS. \quad (4)$$

It is remarkable to note that the motion of the particle is always irrotational ($\boldsymbol{\Omega} = \mathbf{0}$) in the present system. This result can be directly derived from Eq. (4) due to homogeneous mobility. In contrast, an uneven surface mobility $M = M(\theta, \phi)$ would generally produce a rotational motion [38].

As previously mentioned, the solute concentration obeys an advection-diffusion equation

$$\frac{\partial c}{\partial t} + \mathbf{u} \cdot \nabla c = \frac{1}{\text{Pe}} \Delta c, \quad (5)$$

where $\text{Pe} = |\mathcal{A}\mathcal{M}|a/D^2$ is the Péclet number. The concentration field is subject to the fixed-flux isotropic boundary condition

$$\frac{\partial c}{\partial r}(r=1) = -A, \quad (6)$$

where the constant rate $A = \mathcal{A}/|\mathcal{A}| = \pm 1$ is the surface activity of emission ($A > 0$) or consumption ($A < 0$) and fulfills the far-field attenuation condition

$$c(r \rightarrow \infty) = 0. \quad (7)$$

We first note that there exists a trivial stationary solution at all Péclet numbers with an isotropic distribution of solute concentration $c_0(r) = A/r$, zero net flow and motionless translational velocity $\mathbf{U} = \mathbf{0}$. At high Péclet numbers, the nonlinear advective term $\mathbf{u} \cdot \nabla c$ plays an essential role. In that scenario it may lead to a polarization of the concentration around the particle surface when Pe is large enough; hence any infinitesimal perturbation to the immobile state solution $c_0(r)$ will trigger a spontaneous persistent swimming motion. This symmetry-breaking feature was reported in [18], where an axisymmetric constraint was imposed. In the present work we allow the particle to move freely in three-dimensional space and aim to see the emergence of rich dynamics, such as straight, meandering, and chaotic motions at large Péclet numbers. Note that other slightly different models have been adopted for phoretic droplets where in addition to tangential flow [Eq. (2)] a Marangoni effect is taken into account which enters the tangential stress balance. In particular, it is shown that only the model with slip velocity (in contrast to the one involving a Marangoni effect) leads (for the axisymmetric problem) to a chaotic regime, highlighting the inequivalence of the two models [19]. Here we consider the simplest model (only tangential flow is taken into account), which will already reveal a variety of motions, from regular to chaotic. We have also admitted that the chemical activity is assumed to be isotropic, for simplicity.

A. Analytic solution for the velocity field

Since we consider a spherical geometry, the velocity field, which fulfills Eqs. (1)–(3), can be solved analytically by applying Lamb's general solution for squirmers in Stokes flow [39,40] via

the expression of the vector spherical harmonic expansion

$$\begin{aligned}
 u_r &= \sum_{n=1}^{\infty} \sum_{m=0}^n \psi_n(r) P_n^m(\cos \theta) (B_{mn} \cos m\phi + \tilde{B}_{mn} \sin m\phi), \\
 u_\theta &= \sum_{n=1}^{\infty} \sum_{m=0}^n \chi_n(r) \sin \theta P_n^{m'}(\cos \theta) (B_{mn} \cos m\phi + \tilde{B}_{mn} \sin m\phi), \\
 u_\phi &= \sum_{n=1}^{\infty} \sum_{m=0}^n \chi_n(r) \left(\frac{-m P_n^m(\cos \theta)}{\sin \theta} \right) (\tilde{B}_{mn} \cos m\phi - B_{mn} \sin m\phi),
 \end{aligned} \tag{8}$$

where $\psi_1(r) = \frac{4}{3}(1 - \frac{1}{r^3})$ and $\psi_n(r) = \frac{n+1}{r^n}(1 - \frac{1}{r^2})$ for $n \geq 2$, $\chi_1(r) = \frac{2}{3}(-2 - \frac{1}{r^3})$ and $\chi_n(r) = \frac{1}{r^n}(\frac{n-2}{n} - \frac{1}{r^2})$ for $n \geq 2$, P_n^m is the associated Legendre polynomial of degree n and order m , and the prime represents differentiation. The concentration field can also be represented as

$$c(r, \theta, \phi, t) = \sum_{n=1}^{\infty} \sum_{m=0}^n P_n^m(\cos \theta) [c_{mn}(r, t) \cos m\phi + \tilde{c}_{mn}(r, t) \sin m\phi]. \tag{9}$$

Note that the zeroth harmonic mode $n = 0$ vanishes in the above expression due to the far-field condition (7). Matching the slip boundary condition (2) via the usage of Eqs. (8) and (9), we find the coefficients

$$B_{mn} = \frac{Mn}{2} c_{mn}(1, t), \quad \tilde{B}_{mn} = \frac{Mn}{2} \tilde{c}_{mn}(1, t). \tag{10}$$

As we can see, the velocity \mathbf{u} (as well as \mathbf{U}) is given in terms of c at the particle surface and when substituted into Eq. (5) yields a closed nonlinear equation for c .

Given the analytic solution for the velocity field, we can compute the translational phoretic speed (written in Cartesian components) via Eq. (4) as

$$\mathbf{U} = \frac{4}{3} (B_{11} \mathbf{e}_x + \tilde{B}_{11} \mathbf{e}_y - B_{01} \mathbf{e}_z). \tag{11}$$

We immediately see that only the first harmonic modes B_{11} , \tilde{B}_{11} , and B_{01} are responsible for the swimming velocity corresponding to the x , y , and z directions and this allows the phoretic particle to swim along an arbitrary direction in the three-dimensional domain.

B. Brief summary of linear stability analysis

In this section we briefly recall the linear stability analysis [18]. As we mentioned earlier, the trivial stationary solution of the immobile state, $c_0(r) = A/r$, exists at all Péclet numbers. Here we analyze its stability by introducing a perturbation of the form

$$c_1(r, \theta, \phi, t) = \sum_{n=1}^{\infty} \sum_{m=0}^n P_n^m(\cos \theta) [C_{mn}(r, t) \cos m\phi + \tilde{C}_{mn}(r, t) \sin m\phi]. \tag{12}$$

Using the ansatz $c_0 + \epsilon c_1$ and neglecting the higher-order terms in ϵ , we derive a set of differential mode equations [by using Eq. (5) and the above velocity field]

$$\frac{\partial}{\partial t} C_{mn} = AM \frac{n}{2} \frac{\psi_n(r)}{r^2} C_{mn}(1, t) + \frac{1}{\text{Pe}} \left\{ \frac{1}{r^2} \left[\frac{\partial}{\partial r} \left(r^2 \frac{\partial C_{mn}}{\partial r} \right) \right] - \frac{n(n+1)}{r^2} C_{mn} \right\}, \tag{13}$$

$$\frac{\partial}{\partial r} C_{mn}(r=1) = 0, \quad C_{mn}(r \rightarrow \infty) = 0, \tag{14}$$

where all the C_{mn} are decoupled from each other, due to the very nature of linearization. It should be noted that the equation for \tilde{C}_{mn} satisfies exactly the same form of equation and thus is omitted here. In addition, the coefficients of the equation do not depend on m . Therefore, for a given n , all the C_{mn}

are identical and thus we look for eigenmodes of the form $C_{mn} = e^{\sigma_n t} C_n(r)$. The eigenvalue problem reads $\mathcal{L}_n C_n = \sigma_n C_n$, in which \mathcal{L}_n denotes the linear operator on the right-hand side of Eq. (13). The interesting fact is that the velocity in the diffusion equation can be expressed in favor of the concentration field, as reported in other papers [18,19,41].

The first term on the right-hand side of Eq. (13) reflects the effect of advection, while the second term is responsible for the diffusion. It can be seen that the sign of the advection term depends on AM and the coefficient of the diffusion term is always positive. As a result, the advection can be destabilizing (stabilizing) when A and M have the same (opposite) sign, whereas the diffusion term is always stabilizing. Since we look for the potentially unstable modes to the system, we henceforth focus on the case when A and M have the same sign. For definiteness, we set $A = M = 1$.

We first note that the neutral condition for instability corresponds to $\sigma_n = 0$, and our aim is to extract the corresponding condition, satisfied by the control parameter Pe . The critical value for the Péclet number is obtained by solving the differential equation $\mathcal{L}_n C_n^0 = 0$ together with the condition (14).

For the first harmonic mode $n = 1$, we find that the general solution, without imposing the boundary conditions, is given by

$$C_1^0(r) = \left[\left(1 - \frac{Pe}{2}\right)r + \frac{Pe}{6} \left(2 + \frac{1}{r^3}\right) \right] \alpha_1 + \left[\left(1 - \frac{Pe}{2}\right) \frac{1}{r^2} + \frac{Pe}{6} \left(2 + \frac{1}{r^3}\right) \right] \beta_1, \quad (15)$$

where α_1 and β_1 are constants. It can be seen clearly that the first term on the right-hand side blows up as $r \rightarrow \infty$. Therefore, we must have $\alpha_1 = 0$. On the other hand, the fact that the second term approaches a nonzero constant as $r \rightarrow \infty$ indicates the presence of a boundary layer. To obtain a nontrivial solution, a matching between the inner and outer solutions should be performed to fulfill the vanishing boundary condition at infinity (see Refs. [19,42] for further details). Finally, by imposing the boundary condition at $r = 1$, we find that $Pe_1 = 4$ is the critical Péclet number. That is, when $Pe > Pe_1 = 4$, the eigenvalue σ_1 becomes positive so that the stationary solution loses its stability, resulting in a solute polarity [solute excess at one pole and deficit at the opposite pole; see the numerical simulation in Fig. 3(a)], leading to spontaneous swimming motion with a certain velocity along a straight line [recall that only the first mode fixes the swimming speed; see Eqs. (10) and (11)].

For higher modes $n \geq 2$, we obtain

$$C_n^0(r) = \left[\left(1 - \frac{2n+1}{4} Pe\right) r^n + \frac{Pe}{4} \left(\frac{n+1}{r^n} + \frac{n}{r^{n+2}} \right) \right] \alpha_n + \left[\left(1 - \frac{2n+1}{4} Pe\right) \frac{1}{r^{n+1}} + \frac{Pe}{4} \left(\frac{n+1}{r^n} + \frac{n}{r^{n+2}} \right) \right] \beta_n, \quad (16)$$

where α_n and β_n are constants. Again, the first term on the right-hand side of the above expression blows up as $r \rightarrow \infty$. Therefore, we must have $\alpha_n = 0$. The second term approaches zero as $r \rightarrow \infty$, which fulfills automatically the vanishing boundary condition. That is, there is no boundary layer for $n \geq 2$. Here the critical number $Pe_n = 4(n+1)$ is obtained by imposing the boundary condition at $r = 1$, beyond which fluctuations of the second moment (stresslet, $n = 2$) or other higher moments ($n \geq 3$) are exponentially amplified. Thus, the progressive increase of Pe leads to more and more harmonics being unstable. This results in more and more complex dynamics, as seen below. We determine now the maximum growth rate σ_{\max} (or maximum eigenvalue of \mathcal{L}_n) numerically for the first several unstable modes as a function of Pe in Fig. 1. This reproduces the results already presented in [18]. As one can see, the onset of unstable eigenmodes is consistent with the theoretical calculation. In addition, at high Péclet numbers, the amplification of unstable modes is stronger for higher harmonics.

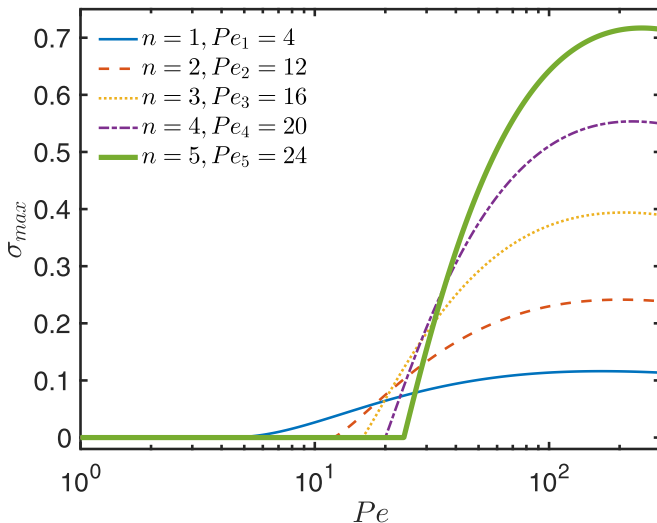


FIG. 1. Maximum growth rate σ_{max} of \mathcal{L}_n as a function of Pe with different modes. Based on the present theoretical prediction [$Pe_1 = 4$ and $Pe_n = 4(n + 1)$ for $n \geq 2$], the spontaneous autophoretic motion occurs when the first swimming mode is activated ($Pe > Pe_1 = 4$).

III. NONLINEAR DYNAMICS

To go beyond the linear analysis presented in the preceding section, we aim to perform a systematic study of the entire diffusiophoretic system (1)–(7). In order to do so, we develop a first-order implicit-explicit time-advancing numerical scheme to discretize Eq. (5). The scheme is outlined as follows: The nonlinear advective term is treated explicitly while the diffusive term is handled implicitly, where the velocity field is given analytically through Eq. (8) and the concentration is decomposed via the spherical harmonic expression (9). This procedure generates a set of 1D partial differential equations for the modes c_{mn} and \tilde{c}_{mn} , which can be solved efficiently using finite-difference discretization in the radial direction. (See Ref. [43] for further details and the convergence validation presented in the Appendix.) Two cases will be studied: (i) a particle constrained to move in an axisymmetric manner and (ii) a free particle moving in three-dimensional space.

A. Results in the axisymmetric case

We first constrain the system to explore only axisymmetric solutions, that is, all the modes with $m \neq 0$ are deliberately set to be zero. In this manner, the particle is allowed to swim along a straight direction, taken to be the z axis, with the locomotion speed denoted by W (z component of \mathbf{U}).

It is found that, for $Pe < Pe_1 = 4$ and as expected from the linear stability, the system recovers the trivial immotile solution regardless of the amplitude of imposed perturbation, whereas when $Pe > Pe_1 = 4$, a spontaneous symmetry-breaking swimming motion is found. This is exactly compatible with the theoretical prediction of the onset of self-propulsion reported in the preceding section. We plot in Fig. 2(a) the speed of the particle as a function of Pe . It can be seen that at $Pe_1 = 4$ the system undergoes a supercritical bifurcation. Remarkably, in Fig. 2(b) we find that the swimming speed $W \propto (Pe - Pe_1)^{1/2}$ close to the onset of bifurcation points. This result is consistent with the prediction in the recently proposed generic model [30,31]. The classical pitchfork behavior is due to finite size [44] in numerical simulations (discussed below). We also find that the nonlinear variation of the phoretic velocity (blue solid line) agrees quantitatively with those (red dots) obtained by

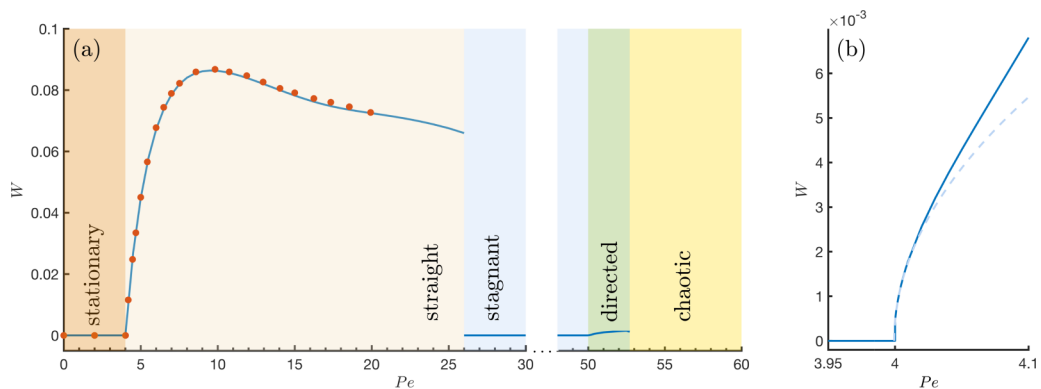


FIG. 2. (a) Bifurcation diagram for the locomotion speed W as a function of Pe under axisymmetric constraint. By increasing Pe , the dynamics of the particle exhibits behaviors such as stationary, straight, stagnant, directed, and chaotic motions. The phoretic velocity obtained by our simulations (blue solid line) agrees quantitatively with the ones (red dots) in [18]. (b) Close-up of (a) around the first critical Péclet number $Pe_1 = 4$. Near $Pe = 4$, the speed W fits well with the dashed curve $1.723 \times 10^{-2}(Pe - Pe_1)^{1/2}$.

Michelin *et al.* [18]. We also note that in this regime where the particle exhibits straight motion, the concentration field shows a cometlike distribution. An example at $Pe = 10$ is shown in Fig. 3(a).

Before proceeding further, an important remark is in order. Morozov and Michelin [45] showed recently that in fact close to the bifurcation point from a nonmotile to a motile state the velocity behaves as $W \sim Pe - Pe_1$ and not as $(Pe - Pe_1)^{1/2}$, as we found above. This result was confirmed by Saha *et al.* [46]. Actually, this finding was also reported earlier by Rednikov *et al.* [41] [see their Eq. (24)]. To be more precise, $|W| \sim Pe - Pe_1$ and the absolute value is a signature of singular behavior. We first note in passing that $|W| \sim Pe - Pe_1$ implies the existence of two symmetric branches of solutions $W \sim \pm(Pe - Pe_1)$ and the bifurcation is not transcritical, as stated in [45], but of pitchfork (albeit singular) nature. This singular behavior is due to the infinite size of the system. In our simulation discretization reintroduces finite-size effects. Even if our domain is formally infinite and mapped onto $(0,1]$ due to the Kelvin inversion (details of numerics are given in [43]), in the transformed coordinate $r = 0$ is excluded (meaning infinity in real space), to avoid numerical singularity. The finite size, even arbitrarily large, regularizes the bifurcation, in that $W \sim (Pe - Pe_1)^{1/2}$. The regularization of the singular pitchfork bifurcation into a classical (regular) pitchfork bifurcation is discussed in detail in [44]. In particular, by focusing on the vicinity of the bifurcation, we prove numerically that the bifurcation is of pitchfork nature [Fig. 2(b)], in agreement with the prediction in [44].

By increasing the Péclet number, the dynamics of the particle transits from motile to another nonmotile and stagnant state ($W = 0$) at $Pe \approx 26$. A similar steady stagnant solution is also observed for chemically active droplets [19]. In this regime, the concentration field is symmetric about $z = 0$, so the swimming velocity equals identically to zero. An example at $Pe = 30$ is shown in Fig. 3(b). Further increasing Pe leads to another transition to directed motion at $Pe \approx 50$. In this regime, the concentration distribution obviously differs from the cometlike one for straight motion, but is closer to the symmetric one for the stagnant solution. An example at $Pe = 51$ is shown in Fig. 3(c). Note that in Fig. 3(c) the concentration has a very small front-back asymmetry and the resulting speed is quite low.

Remarkably, it is found that the directed motion turns into periodic motion when $Pe \gtrsim 52.64$, and the system undergoes a period-doubling cascade as Pe increases in the region $52.64 \lesssim Pe \lesssim 52.72$. This period-doubling cascade shows an accumulation point, corresponding to the transition to chaos. The period-doubling cascade is one of the three classical scenarios of the transition to chaos (the two others being intermittency and quasiperiodicity). With the help of extensive and

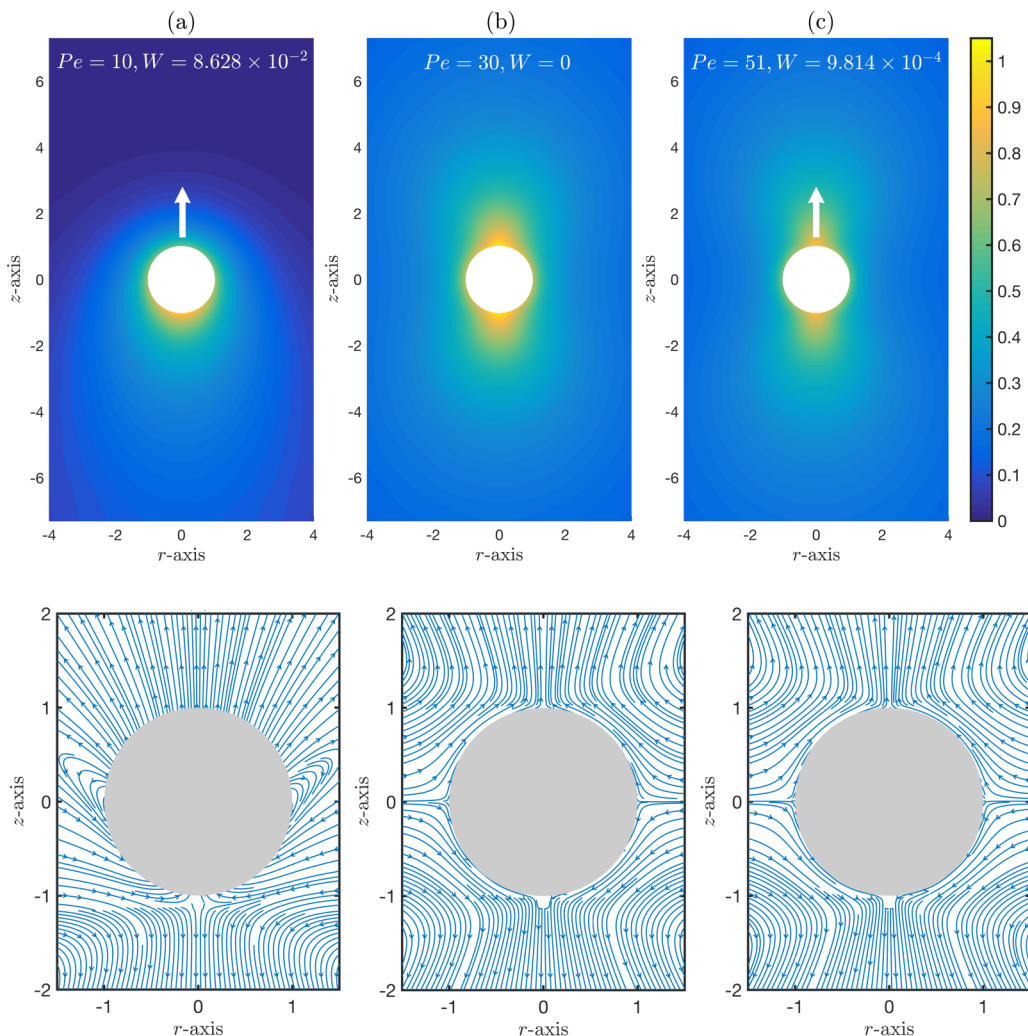


FIG. 3. Shown on top is the concentration distribution denoted using the color code for symmetric-breaking solutions in (a) straight ($Pe = 10$ and $W = 8.628 \times 10^{-2}$), (b) stagnant ($Pe = 30$ and $W = 0$), and (c) directed ($Pe = 51$ and $W = 9.814 \times 10^{-4}$) regimes. The white arrow denotes the swimming direction. Shown on the bottom are the corresponding streamlines.

careful numerical computations, we can describe five subwindows supporting the occurrence of the period-doubling cascade and the beginning of accumulation of critical points for successive period-doubling bifurcations. For brevity of the description, we only give the representative results for each subwindow phase-plane diagram ($W, dW/dt$). We start by setting $Pe = 52.64$, corresponding to the first subwindow. Due to the periodicity of the solution, the phase portrait forms a closed curve with time period $T = 159.22$ [see Fig. 4(a)]. Next the value of Pe is increased to 52.67, which lies in the second subwindow. The topology of the phase curve shown in Fig. 4(b) appears to change, while a new branch can be clearly seen. In this case the period $T = 318.125$. For $Pe = 52.70$, corresponding to the third subwindow, the phase diagram is given in Fig. 4(c), where a new discernible branch is generated with the period $T = 632.988$. In the fourth subwindow, we set $Pe = 52.71$ and obtain the period $T = 1264.69$ [see Fig. 4(d)]. It can also be clearly seen in Figs. 4(a)–(c) that the distance between two successive critical values of Pe becomes smaller and

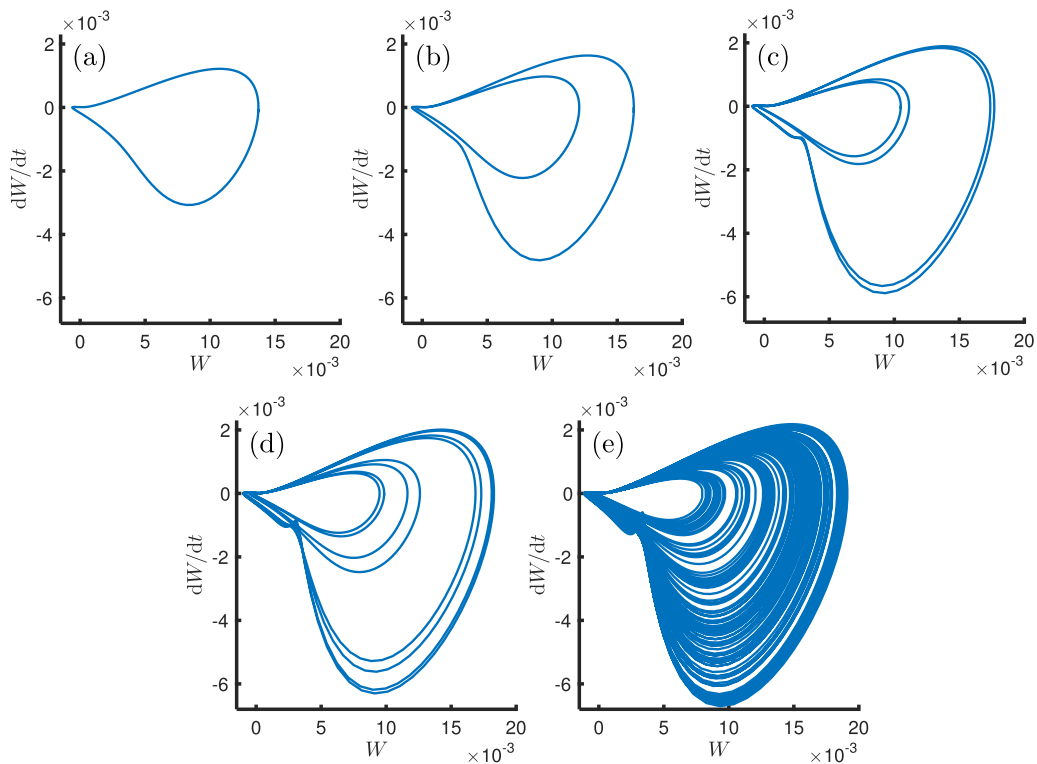


FIG. 4. Phase-plane diagram ($W, dW/dt$) at (a) $Pe = 52.64$ and $T = 159.22$, (b) $Pe = 52.67$ and $T = 318.125$, (c) $Pe = 52.70$ and $T = 632.988$, (d) $Pe = 52.71$ and $T = 1264.69$, and (e) $Pe = 52.72$ and $T = \infty$. The time periods T of the solution undergo a period-doubling cascade as Pe is increased in the region $52.64 \lesssim Pe \lesssim 52.72$.

smaller, which shows a generic feature of a subharmonic cascade. The final example corresponds to $Pe = 52.72$ [the fifth subwindow; see Fig. 4(e)]. In this case the dynamics shows a strange attractor, characteristic of chaotic motion. As previously mentioned the subharmonic cascade occurs in the very narrow region $52.64 \lesssim Pe \lesssim 52.72$, so these time periodic motions can be sensitive to a small increment of Pe . We therefore run a series of numerical simulations to confirm the numerical validity of these results. It shows that the time periodic numerical solutions converge when refining spatial or temporal step size (see the Appendix). This guarantees the correctness of the observed scenarios and the convergence of our proposed numerical scheme in [43].

To further characterize the solution behavior in this regime, we illustrate, with a numerical simulation at $Pe = 54$, the behavior of the MSD and the corresponding swimming speed in Fig. 5. It can be seen that the swimming speed exhibits an apparent random rectilinear motion, while the average value of the velocity highlights the tendency to swim along a certain direction (either positive or negative z axis), and this results in the MSD being proportional to τ^2 at long times. Notably, the quadratic behavior of MSD is also found for the chaotic swimming of active droplets under the axisymmetric assumption in [19]. However, no directed motion is reported after the stagnant one. This is probably due to the difference in models (a rigid particle here and a droplet in Ref. [19]). *A priori*, since the particle undergoes chaos, we could have expected to have a nonballistic motion (for example, normal and abnormal diffusion). The origin of this ballistic behavior may be understood as follows. Due to axisymmetry, the particle moves in a given direction in the directed motion (preceding chaos). The two opposite directions are equally good candidates. However, given an initial condition, the particle will select one definite direction (and not the other). When chaos

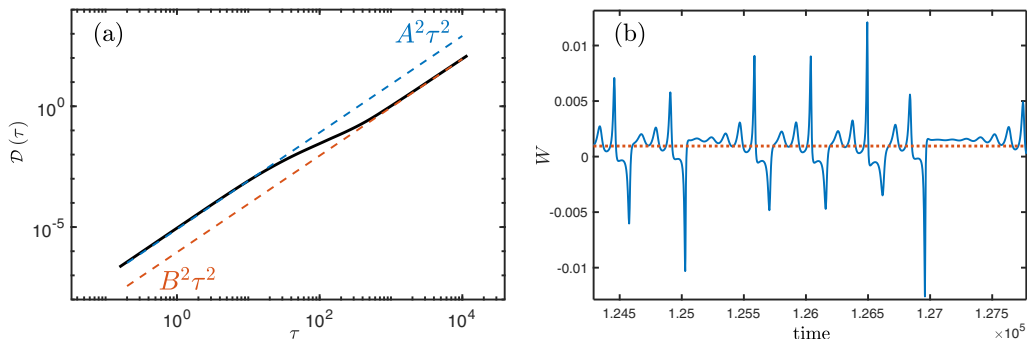


FIG. 5. (a) Mean-square displacement for the particle trajectory at $Pe = 54$ in the chaotic regime, with a fit with $A^2\tau^2$ at short time and $B^2\tau^2$ at long time. Here $A = 2.857 \times 10^{-3}$ and $B = 9.494 \times 10^{-4}$. (b) Profile of swimming speed W in a certain time interval. The dotted line shows the value of B .

takes place, the particle goes back and forth in its own frame. In the laboratory frame, the particle has on the average a definite directed motion along, say the positive z axis. Simulations show that MSD is made of two successive quadratic regimes in time that can be interpreted as short-time and long-time ballistic regimes.

At short enough times the particle undergoes a ballistic motion associated with velocity $|W(t)|$. More precisely, we define

$$A^2 = \frac{1}{N} \sum_{i=1}^N W_i^2, \quad (17)$$

where W_i is the speed at different time steps t_i . At short times the particle makes back and forth motion with a negligible net forward motion [measured by $(\sum_i W_i)^2$] so that the mean-square displacement is dominated by $\sum_i W_i^2$. In that case we expect $\mathcal{D} \sim A^2\tau^2$. At long times the particle makes a back and forth motion but makes a significant net forward motion which is dominated by $(\sum_i W_i)^2$. We define

$$B^2 = \left(\frac{1}{N} \sum_{i=1}^N W_i \right)^2 \quad (18)$$

and we expect $\mathcal{D} \sim B^2\tau^2$. The results of these two ballistic motion are shown in Fig. 5, showing remarkable agreement with the full numerical simulation. The chaotic back and forth motion is related to a chaotic oscillation of concentration polarity around the bead. As shown above, only the first harmonic contributes to the swimming speed. Therefore, in order to make the polarity oscillation more visible, we have projected the concentration field onto the first harmonic. We show in the Supplemental Material [47] a movie highlighting the chaotic behavior of the comet.

B. Results in three dimensions

Now we turn our attention to the case where the particle is free to move in three-dimensional space. We plot the bifurcation diagram for the phoretic velocity $\|\mathbf{U}\|$ as a function of Pe in Fig. 6. It can be seen that, as expected, the trivial stationary solution loses its stability when $Pe > Pe_1 = 4$. Once the instability threshold is reached, i.e., the first mode is activated ($n = 1$), a symmetry-breaking solution takes place so that the particle is able to persistently propel itself along an arbitrary direction with constant velocity that leads to a particle trajectory of the form $\mathbf{X}(t) = \mathbf{U}_0 t + \mathbf{X}(0)$, where \mathbf{U}_0 is a constant vector. In such a scenario, the concentration field of the particle shows the cometlike pattern [see Fig. 3(a)], leading to a nonzero concentration gradient on the particle surface.

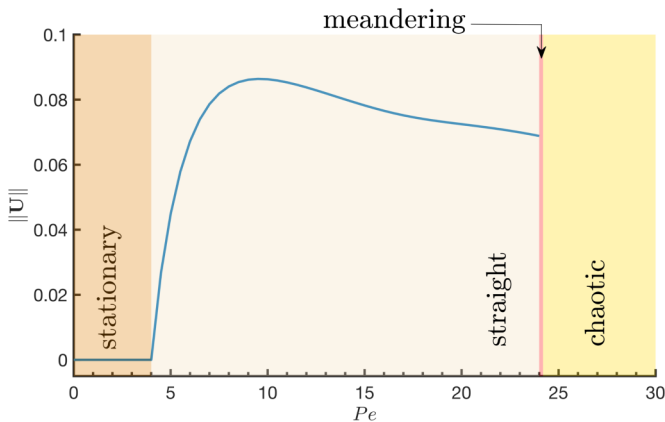


FIG. 6. Bifurcation diagram for the locomotion speed $\|\mathbf{U}\|$ versus Pe in three dimensions. By increasing Pe , the dynamics of particle exhibits behaviors such as stationary, straight, meandering, and chaotic motions.

Also, the magnitude of $\|\mathbf{U}\|$ in the regime of straight motion is obviously identical to that obtained under the axisymmetric assumption (see Fig. 6).

It is interesting to see that, different from the axisymmetric case, the directed swimming solution loses its stability (a secondary instability) at $Pe \approx 24.1$ in favor of a meandering motion. In this regime, the swimming velocity is no longer a constant but periodically oscillates in time. The particle trajectory can be written as $\mathbf{X}(t) = \mathbf{U}_0 t + \mathbf{U}_1 F(t) + \mathbf{X}(0)$, where \mathbf{U}_0 and \mathbf{U}_1 are constant vectors and $F(t)$ is a periodic function. An example of the meandering particle motion at $Pe = 24.1$ is shown in Fig. 7. We should also point out that the trajectory is in fact two dimensional, that is, the particle's trajectory lies on a two-dimensional affine subspace of \mathbb{R}^3 . So the meandering motion in this regime is entirely planar.

Soon, at $Pe \geq 24.2$, the particle quits the meandering motion and enters directly into an apparent chaotic regime. This reveals that the effect of the nonlinear advective term becomes pronounced while the growth of the high harmonic modes is triggered. The activation of this harmonic mode contributes to the appearance of an irregular chaotic burst, as shown in Fig. 8, which represents the swimming speed of the particle close to the transition towards chaos. As the Péclet number is increased further the occurrence of the chaotic burst becomes more frequent until $Pe \simeq 24.5$, where the whole trajectory becomes erratic in time, via the intermittency scenario. As a demonstration for solutions in the chaotic regime, we perform a simulation at $Pe = 24.5$ where the particle exhibits an apparently random motion, as shown in Fig. 9(a), and we quantify this random walk by measuring the MSD in Fig. 9(b). At short times the particle produces a persistent run-and-tumble-like motion and the MSD curve is then quadratic in time. At longer times, a decorrelation process due to chaotic turns takes place with MSD proportional to τ , which is typical of a classical random walk. This

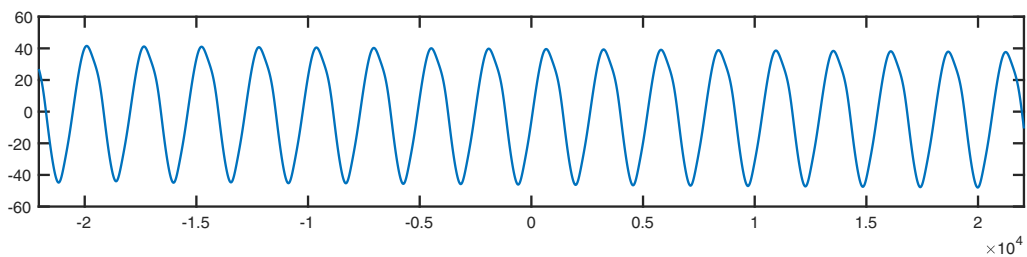


FIG. 7. Particle trajectory at $Pe = 24.1$ showing a meandering straight motion.

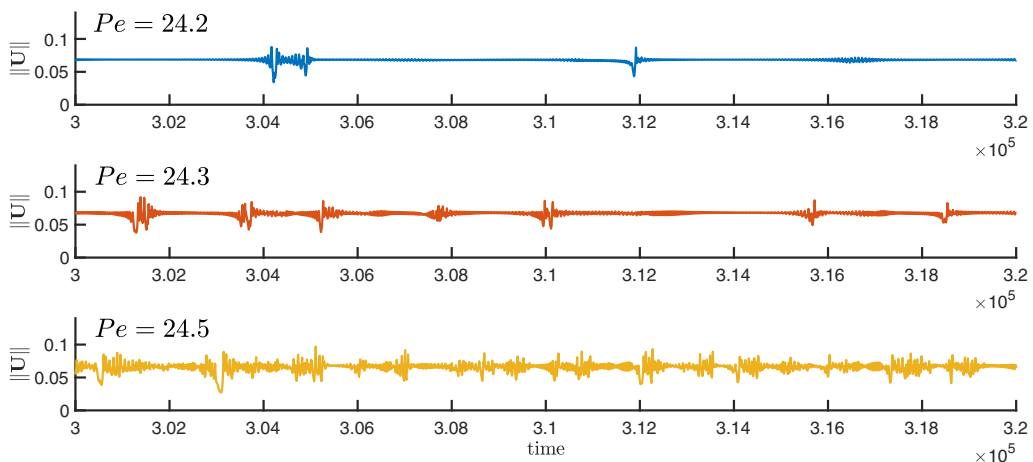


FIG. 8. Profile of the propulsion speed $\|\mathbf{U}\|$ as a function of time at $Pe = 24.2, 24.3,$ and 24.5 . As Pe is increased the chaotic bursts become more frequent, until at $Pe \simeq 24.5$ where the speed becomes erratic in time.

demonstration gives evidence that the complicated swimming motion can arise under the minimal version of dynamics such as in this system, provided by a strong nonlinearity induced from the advective component. This result agrees with our previous simulation in two dimensions [29], highlighting its robustness.

Note that some quasi-2D experiments (Hele-Shaw geometry or a confined microfluidic device) [33,34] reported on a self-avoiding walk, where the concentration emitted at earlier times by the particle has a long-lived period so that at the next passage at a later time the particle avoids its own trail. Other experiments [35] did not observe, however, a self-avoiding walk, but rather a diffusionlike random walk, as found here. This highlights the fact that the self-avoiding walk is not the rule. The concentration trail decays with time, with a decay time of order $1/Dq^2$, where q is a wave number of order $1/a$. We have thus a typical time a^2/D . The particle (in the chaotic regime) moves with velocity W of order $D(Pe - Pe_1)/a$, and its time to travel a persistent length L is of order L/W . The decay time is of order a^2/D , while the travel time is of order $aL/D Pe$ (in the chaotic regime $Pe \gg Pe_1$). In the chaotic regime $Pe \sim 25$ and the decay time is smaller provided $L/a > 25$. The typical persistent length is of order of at least $100a$, meaning that the decay time is shorter than the travel time. Thus on the next passage of the particle at previously visited sites

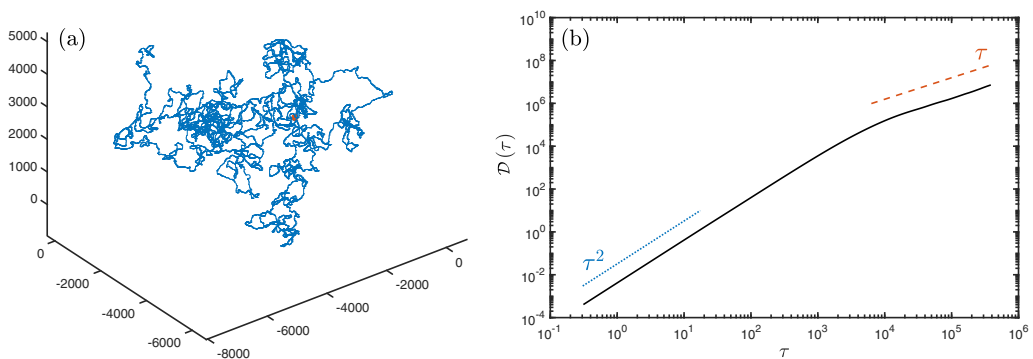


FIG. 9. (a) Particle trajectory at $Pe = 24.5$ (the red dot marks the origin). (b) Corresponding MSD (solid line) showing a classical random walk as normal diffusion.

the concentration trail would have significantly decayed. A more precise estimate for the travel time is to use the computed velocity $0.06|\mathcal{AM}|/D$ (recall that velocity in Fig. 6 is rescaled by $|\mathcal{AM}|/D$) so that the travel time is of order $aL/0.06D\text{Pe}$, to be compared to a^2/D . Taking $\text{Pe} = 25$, we find that the travel time is longer than the decay time if $L/a \gg 1.5$, which is safely fulfilled. For significantly larger Pe , the travel time may be reduced so that self-avoidance may emerge. Note also that the above-mentioned experiments where a self-avoiding walk is observed [33,34] are quasi-2D (confined swimming), a fact which may favor self-avoidance, in contrast to our simulation, which is performed in three dimensions. In that case the probability of successive passages is very low, making the exponent of the MSD in the self-avoiding walk close to that of a classical random walk (equal to about 1.2 in three dimensions, to be compared to about 1.5 in two dimensions) [48]. It will be an interesting task for future work to reanalyze the 2D simulation in light of these observations.

IV. CONCLUSION

In this paper we have shown that a complex dynamics, such as directed, stagnant, meandering, or chaotic propulsion, arises for an individual spherical particle powered by a chemical species. A minimal and fully three-dimensional model was proposed to mimic the diffusiophoretic system. We took advantage of Lamb's general solution to find the analytic velocity field generated by a surface slip flow with arbitrary concentration coverage. Given an isotropic fixed-flux boundary condition (emission or consumption of concentration) and constant mobility, our linear stability analysis revealed that the nonmotile stationary solution loses its stability when advection of concentration is sufficiently strong, i.e., beyond the first critical Péclet number $\text{Pe}_1 = 4$. We further derived the critical Péclet number for higher harmonic modes.

More specifically, under the axisymmetric constraint, we found that the only nonlinear ingredient of the model (concentration advection) leads to multiple types of spontaneous swimming locomotion. When the first harmonic mode is activated ($\text{Pe} > \text{Pe}_1$), the self-propulsion straight motion is observed in which the polarization of concentration occurs. A strong advection may destabilize this steady self-propelling swimming and spontaneously stop the locomotion with a symmetric net flow. If advection is strengthened further (i.e., increasing Pe), the symmetric state loses its stability and the particle turns to a directed motion with a slow speed. Strengthening the advective component even further, we found that the directed motion experienced a subharmonic cascade and enters chaotic oscillation, which was characterized by random reversal of the propulsion direction (thus the particle swims back and forth), and the MSD behaves quadratically in this chaotic regime. Chaos was found here to occur via a subharmonic cascade. In contrast, in fully three-dimensional space, another bifurcation scenario occurs. Namely, the straight motion turns into a periodic meandering motion, and this motion is only found in a very narrow region for $\text{Pe} \sim 24.1$, before entering a chaotic regime. Different from the axisymmetric case, the chaotic bursts of the velocity become more and more frequent as Pe increases, until the trajectory becomes fully chaotic, via the intermittency scenario. The erratic trajectory shows a diffusive nature where the MSD reaches a linear function at long times.

Throughout this paper, we considered the simple case of constant chemical activity and mobility, which always results in irrotational phoretic motion. Appropriate models may be designed to lead to pure translation, pure rotation, circular or generally helical motion [38], which is left for future study. This general setup should serve as a guide for designing arbitrary phoretic spheres with desired locomotion properties.

Finally, besides the phoretic particles discussed here, other systems, such as mammalian cells, are known to swim in a fluid [3–6]. In this case, cell motility is assisted by actin and myosin dynamics [5,49,50]. Actin polymerizes at the cell front (serving as a sink) and depolymerizes at the back, whereas myosin exerts contractile stress on the cell cortex, affecting thus the cortex stress (very much like the Marangoni effect). We thus expect similar complex dynamics found here to occur within these systems as well. Morozov [51] considered a more general model where the

chemical activity depends on the particle surface surfactant concentration, as well an adsorption current depending on the micellar concentration. This led to the discovery of multistable regimes where a moving solution coexists with a stagnant solution showing an extensional symmetric flow. It will be an interesting task for future investigations to see how this type of model refinement would affect (besides multistability [51]) the overall features reported here.

ACKNOWLEDGMENTS

C.M. is grateful to Centre National d'Etudes Spatiales for financial support and access to data of microgravity and C.M. and S.R. are grateful to the French-German university program "Living Fluids" (Grant No. CFDA-Q1-14) for financial support. W.-F.H. and T.-S.L. acknowledge support from Ministry of Science and Technology, Taiwan, under research Grants No. MOST-109-2115-M-008-014-MY2 and No. MOST-109-2115-M-009-006-MY2, respectively.

APPENDIX

Here we present the convergence validation of the present numerical solver. Following [43], we apply Kelvin's inversion with $\bar{r} = 1/r$ so that the spatial domain is bounded, $\bar{r} \in (0, 1]$. We choose $Pe = 10$ with initial concentration $c(t = 0) = \frac{1}{r} - \frac{1}{10} \exp[-(r - 1)^2] P_1^1(\cos \theta)(\cos \phi + \sin \phi)$ and perform the simulation up to $T = 10$ (the flow field is developing to straight motion). In each simulation, we fix 32 and 64 points in the polar and azimuthal directions, respectively (in spherical harmonic expansion). Denoting the radial mesh width by $\Delta\bar{r}$ and setting the time step size $\Delta t = \Delta\bar{r}$, the results of the convergence study are reported in Fig. 10. As one can see, the swimming speed $\|\mathbf{U}\|$ converges to a certain value when refining $\Delta\bar{r}$ [Fig. 10(a)], while, as expected, the convergence rate is roughly first order [Fig. 10(b)].

We also validate the convergence in both spatial and temporal domains for solutions in the period-doubling regime. We choose $Pe = 52.64$ and run a series of simulations with fixed mesh size $\Delta\bar{r} = 0.03125$ and different time steps Δt . As can be seen in Fig. 11, the periodic motion can indeed be captured in each simulation; we can also observe that the phase portrait $(W, dW/dt)$ tends to converge to a limit cycle along with the convergent time period T when refining the time step size. On the other hand, we perform the convergence study of spatial size as follows. Note that all results in Fig. 4 are obtained by using $\Delta\bar{r} = 0.03125$ and $\Delta t = 0.1562$. While using the finer spatial mesh width $\Delta\bar{r} = 0.015625$, Fig. 12 shows that the period-doubling cascade can be reproduced but with slightly different Pe values. (Note that the boundaries, or critical Pe values, of subwindows in this regime can vary a little bit due to the error from numerical discretization.) The above study demonstrates the validation for the convergence of the numerical method.

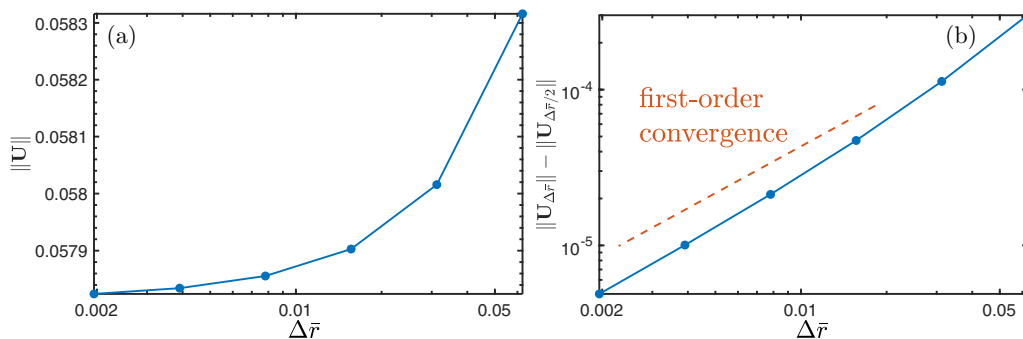


FIG. 10. (a) Swimming speed $\|\mathbf{U}\|$ at different mesh sizes. (b) Consecutive error $\|\mathbf{U}_{\Delta\bar{r}}\| - \|\mathbf{U}_{\Delta\bar{r}/2}\|$.

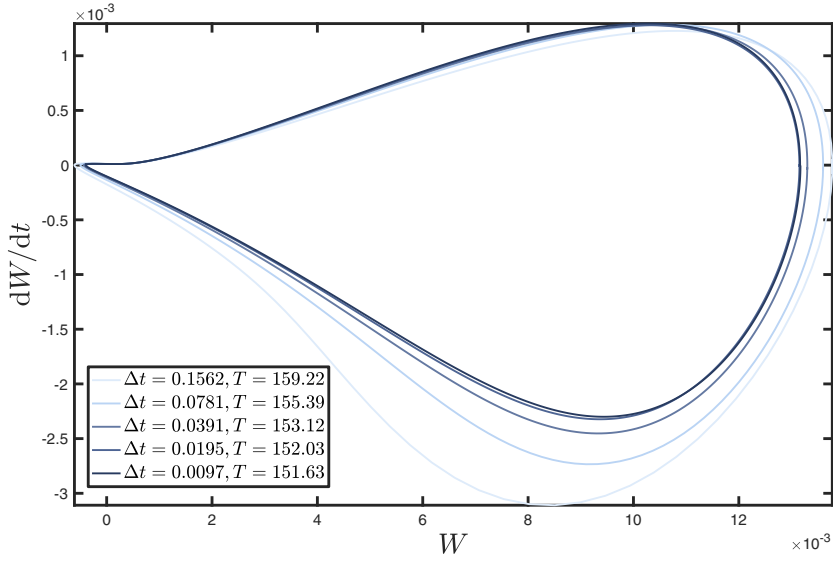


FIG. 11. Phase-plane diagram ($W, dW/dt$) with $Pe = 52.64$ and $\Delta\bar{r} = 0.03125$.

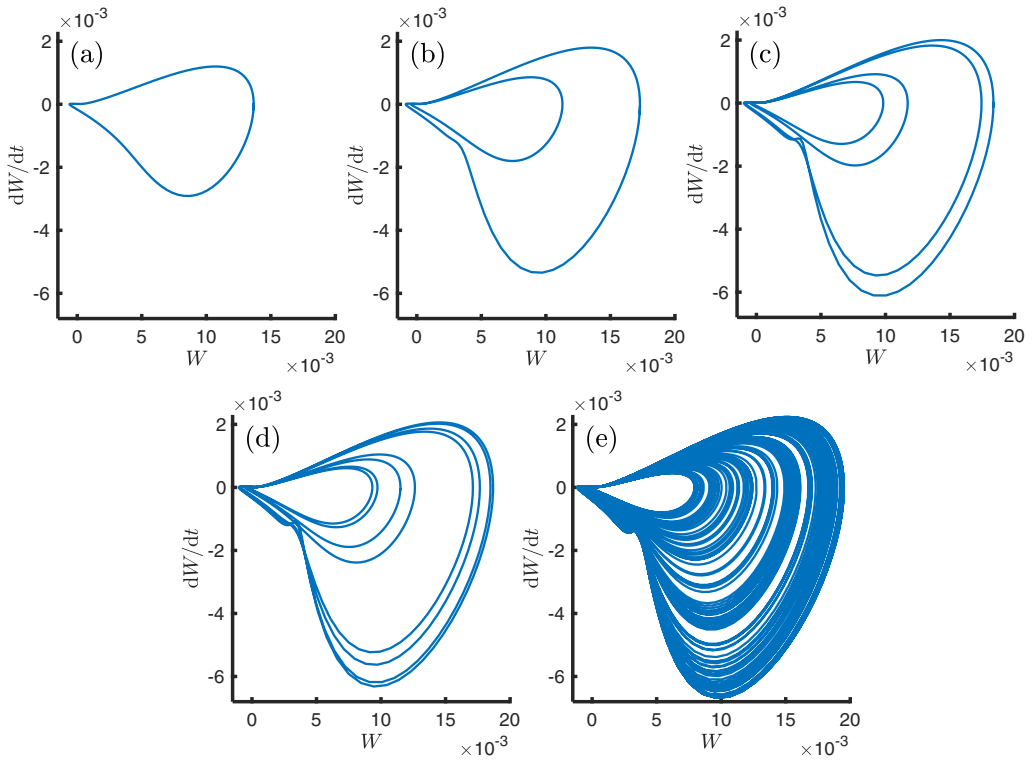


FIG. 12. Phase-plane diagram ($W, dW/dt$) at (a) $Pe = 53.10$ and $T = 160.00$, (b) $Pe = 53.15$ and $T = 318.59$, (c) $Pe = 53.17$ and $T = 635.31$, (d) $Pe = 53.176$ and $T = 1270.19$, and (e) $Pe = 53.20$ and $T = \infty$.

- [1] E. Lauga and T. R. Powers, The hydrodynamics of swimming microorganisms, *Rep. Prog. Phys.* **72**, 096601 (2009).
- [2] M. C. Marchetti, J.-F. Joanny, S. Ramaswamy, T. B. Liverpool, J. Prost, M. Rao, and R. A. Simha, Hydrodynamics of soft active matter, *Rev. Mod. Phys.* **85**, 1143 (2013).
- [3] N. P. Barry and M. S. Bretscher, Dictyostelium amoebae and neutrophils can swim, *Proc. Natl. Acad. Sci. USA* **107**, 11376 (2010).
- [4] P. R. O’Neill, J. A. Castillo-Badillo, X. Meshik, V. Kalyanaraman, K. Melgarejo, and N. Gautam, Membrane flow drives an adhesion-independent amoeboid cell migration mode, *Dev. Cell* **46**, 9 (2018).
- [5] A. Farutin, J. Etienne, C. Misbah, and P. Récho, Crawling in a Fluid, *Phys. Rev. Lett.* **123**, 118101 (2019).
- [6] L. Aoun, P. Negre, A. Farutin, N. Garcia-Seyda, M. S. Rivzi, R. Galland, A. Michelot, X. Luo, M. Biarnes-Pelicot, C. Hivroz, S. Rafai, J.-B. Sibaret, M.-P. Valignat, C. Misbah, and O. Theodoly, Amoeboid swimming is propelled by molecular paddling in lymphocytes, *Biophys. J.* **119**, 1157 (2020).
- [7] M. Polin, I. Tuval, K. Drescher, J. P. Gollub, and R. E. Goldstein, Chlamydomonas swims with two “gears” in a eukaryotic version of run-and-tumble locomotion, *Science* **325**, 487 (2009).
- [8] S. Rafai, L. Jibuti, and P. Peyla, Effective Viscosity of Microswimmer Suspensions, *Phys. Rev. Lett.* **104**, 098102 (2010).
- [9] P. J. A. Janssen and M. D. Graham, Coexistence of tight and loose bundled states in a model of bacterial flagellar dynamics, *Phys. Rev. E* **84**, 011910 (2011).
- [10] L. Turner, W. S. Ryu, and H. C. Berg, Real-time imaging of fluorescent flagellar filaments, *J. Bacteriol.* **182**, 2793 (2000).
- [11] M. L. Ginger, N. Portman, and P. G. McKean, Swimming with protists: Perception, motility and flagellum assembly, *Nat. Rev. Microbiol.* **6**, 838 (2008).
- [12] S. Jana, S. H. Um, and S. Jung, Paramecium swimming in capillary tube, *Phys. Fluids* **24**, 041901 (2012).
- [13] S. Pinner and E. Sahai, Imaging amoeboid cancer cell motility in vivo, *J. Microsc.* **231**, 441 (2008).
- [14] T. Lämmermann and M. Sixt, Mechanical modes of ‘amoeboid’ cell migration, *Curr. Opin. Cell Biol.* **21**, 636 (2009).
- [15] R. Poincloux, O. Collin, F. Lizárraga, M. Romao, M. Debray, M. Piel, and P. Chavrier, Contractility of the cell rear drives invasion of breast tumor cells in 3D Matrigel, *Proc. Natl. Acad. Sci. USA* **108**, 1943 (2011).
- [16] A. Farutin, S. Rafai, D. K. Dysthe, A. Duperray, P. Peyla, and C. Misbah, Amoeboid Swimming: A Generic Self-Propulsion of Cells in Fluids by Means of Membrane Deformations, *Phys. Rev. Lett.* **111**, 228102 (2013).
- [17] H. Wu, A. Farutin, W.-F. Hu, M. Thiebaud, S. Rafai, P. Peyla, M.-C. Lai, and C. Misbah, Amoeboid swimming in a channel, *Soft Matter* **12**, 7470 (2016).
- [18] S. Michelin, E. Lauga, and D. Bartolo, Spontaneous autophoretic motion of isotropic particles, *Phys. Fluids* **25**, 061701 (2013).
- [19] M. Morozov and S. Michelin, Nonlinear dynamics of a chemically-active drop: From steady to chaotic self-propulsion, *J. Chem. Phys.* **150**, 044110 (2019).
- [20] M. Schmitt and H. Stark, Swimming active droplet: A theoretical analysis, *Europhys. Lett.* **101**, 44008 (2013).
- [21] H. S. Jennings, On the significance of spiral swimming of organisms, *Am. Nat.* **35**, 369 (1901).
- [22] V. B. Shenoy, D. T. Tambe, A. Prasad, and J. A. Theriot, A kinematic description of the trajectories of *Listeria monocytogenes* propelled by actin comet tails, *Proc. Natl. Acad. Sci. USA* **104**, 8229 (2007).
- [23] I. H. Riedel, K. Kruse, and J. Howard, A self-organized vortex array of hydrodynamically entrained sperm cells, *Science* **309**, 300 (2005).
- [24] C. Krüger, G. Klös, C. Bahr, and C. C. Maass, Curling Liquid Crystal Microswimmers: A Cascade of Spontaneous Symmetry Breaking, *Phys. Rev. Lett.* **117**, 048003 (2016).
- [25] H. Löwen, Chirality in microswimmer motion: From circle swimmers to active turbulence, *Eur. Phys. J.: Spec. Top.* **225**, 2319 (2016).
- [26] M. Suga, S. Suda, M. Ichikawa, and Y. Kimura, Self-propelled motion switching in nematic liquid crystal droplets in aqueous surfactant solutions, *Phys. Rev. E* **97**, 062703 (2018).

- [27] N. Narinder, C. Bechinger, and J. R. Gomez-Solano, Memory-Induced Transition from a Persistent Random Walk to Circular Motion for Achiral Microswimmers, *Phys. Rev. Lett.* **121**, 078003 (2018).
- [28] Z. Izri, M. N. Van Der Linden, S. Michelin, and O. Dauchot, Self-Propulsion of Pure Water Droplets by Spontaneous Marangoni-Stress-Driven Motion, *Phys. Rev. Lett.* **113**, 248302 (2014).
- [29] W. F. Hu, T. S. Lin, S. Rafai, and C. Misbah, Chaotic Swimming of Phoretic Particles, *Phys. Rev. Lett.* **123**, 238004 (2019).
- [30] C. Misbah, M. S. Rizvi, W. F. Hu, T. S. Lin, S. Rafai, and A. Farutin, Universal trajectories of motile particles driven by chemical activity, [arXiv:2112.13801](https://arxiv.org/abs/2112.13801).
- [31] A. Farutin, M. S. Rizvi, W. F. Hu, T. S. Lin, S. Rafai, and C. Misbah, Motility and swimming: Universal description and generic trajectories, [arXiv:2112.12287](https://arxiv.org/abs/2112.12287).
- [32] Y. Chen, K. L. Chong, L. Liu, R. Verzicco, and D. Lohse, Instabilities driven by diffusiophoretic flow on catalytic surfaces, *J. Fluid Mech.* **919**, A10 (2021).
- [33] B. V. Hokmabad, R. Dey, M. Jalaal, D. Mohanty, M. Almukambetova, K. A. Baldwin, D. Lohse, and C. C. Maass, Emergence of Bimodal Motility in Active Droplets, *Phys. Rev. X* **11**, 011043 (2021).
- [34] C. Jin, C. Krüger, and C. C. Maass, Chemotaxis and autochemotaxis of self-propelling droplet swimmers, *Proc. Natl. Acad. Sci. USA* **114**, 5089 (2017).
- [35] A. Izzet, P. G. Moerman, P. Gross, J. Groenewold, A. D. Hollingsworth, J. Bibette, and J. Brujic, Tunable Persistent Random Walk in Swimming Droplets, *Phys. Rev. X* **10**, 021035 (2020).
- [36] W. F. Paxton, K. C. Kistler, C. C. Olmeda, A. Sen, S. K. St. Angelo, Y. Cao, T. E. Mallouk, P. E. Lammert, and V. H. Crespi, Catalytic nanomotors: Autonomous movement of striped nanorods, *J. Am. Chem. Soc.* **126**, 13424 (2004).
- [37] H. A. Stone and A. D. T. Samuel, Propulsion of Microorganisms by Surface Distortions, *Phys. Rev. Lett.* **77**, 4102 (1996).
- [38] M. Lisicki, S. Reigh, and E. Lauga, Autophoretic motion in three dimensions, *Soft Matter* **14**, 3304 (2018).
- [39] J. L. Anderson, Colloid transport by interfacial forces, *Annu. Rev. Fluid Mech.* **21**, 61 (1989).
- [40] O. S. Pak and E. Lauga, Generalized squirming motion of a sphere, *J. Eng. Math.* **88**, 1 (2014).
- [41] A. Y. Rednikov, Y. S. Ryazantsev, and M. G. Velarde, Drop motion with surfactant transfer in a homogeneous surrounding, *Phys. Fluids* **6**, 451 (1994).
- [42] A. Acrivos and T. D. Taylor, Heat and mass transfer from single spheres in stokes flow, *Phys. Fluids* **5**, 387 (1962).
- [43] T.-S. Lin, W.-F. Hu, and C. Misbah, A direct poisson solver in spherical geometry with an application to diffusiophoretic problems, *J. Comput. Phys.* **409**, 109362 (2020).
- [44] A. Farutin and C. Misbah, Singular bifurcations: A regularization theory, [arXiv:2112.12094](https://arxiv.org/abs/2112.12094).
- [45] M. Morozov and S. Michelin, Self-propulsion near the onset of Marangoni instability of deformable active droplets, *J. Fluid Mech.* **860**, 711 (2019).
- [46] S. Saha, E. Yariv, and O. Schnitzer, Isotropically active colloids under uniform force fields: From forced to spontaneous motion, *J. Fluid Mech.* **916**, A47 (2021).
- [47] See Supplemental Material at <http://link.aps.org/supplemental/10.1103/PhysRevFluids.7.034003> for a movie highlighting the chaotic behavior of the comet.
- [48] S. Havlin and D. Ben-Avraham, Theoretical and numerical study of fractal dimensionality in self-avoiding walks, *Phys. Rev. A* **26**, 1728 (1982).
- [49] R. J. Hawkins, R. Poincloux, O. Bénichou, M. Piel, P. Chavrier, and R. Voituriez, Spontaneous contractility-mediated cortical flow generates cell migration in three-dimensional environments, *Biophys. J.* **101**, 1041 (2011).
- [50] A. C. Callan-Jones, V. Ruprecht, S. Wieser, C. P. Heisenberg, and R. Voituriez, Cortical Flow-Driven Shapes of Nonadherent Cells, *Phys. Rev. Lett.* **116**, 028102 (2016).
- [51] M. Morozov, Adsorption inhibition by swollen micelles may cause multistability in active droplets, *Soft Matter* **16**, 5624 (2020).